Temporal Dependency of Air Entrainment to Liquid Flow Rate Variations For Gasoline Direct Injection Sprays

Delay G.[(1)]✉, Bazile R. [(1)], Charnay G. [(1)], Nuglisch H.J. [(2)]
[(1)] Institut de Mécanique des Fluides de Toulouse, Allée Camille Soula, EEC, 31400 Toulouse, France.
[(2)] SIEMENS VDO Automotive, bp 1149, 1 avenue Paul Ourliac, 31036 Toulouse cedex 1, France
Corresponding author: delay@imft.fr

ABSTRACT

The present work deals with the transient analysis of two typical quantities of an injector and how determining them by experimental methods. First of all, the instantaneous liquid flow rate is to be studied because it rules the whole dynamic of the combustion (droplets diameter, velocity and concentration). Laser-based experimentations have been set up to study those quantities over a wide functioning range (varying injector type, injection pressure, duration and frequency). On one hand, Laser Doppler Velocimetry (LDV) measurements and an analytical approach of periodical pulsated laminar flows (Durst & al. 1996, Lambossy 1952, Bopp & al. 1990, Ismailov & al. 1999, 1999, Durst & al. 1996) are used to determine the instantaneous flow rate from measurements of the centerline velocity in the pipe feeding the injector (Fig.1a). On the other, measurements of the air entrained by the spray is achieved using Particle Image Velocimetry on Fluorecent dye (F-PIV). Transient analysis is then carried out to evaluate liquid flow rate oscillation influence on transient air entrainment. It seems that the same frequencies are monitored upstream the injector in the gasoline system and downstream in the air entrainment by the spray (Fig. 1b).

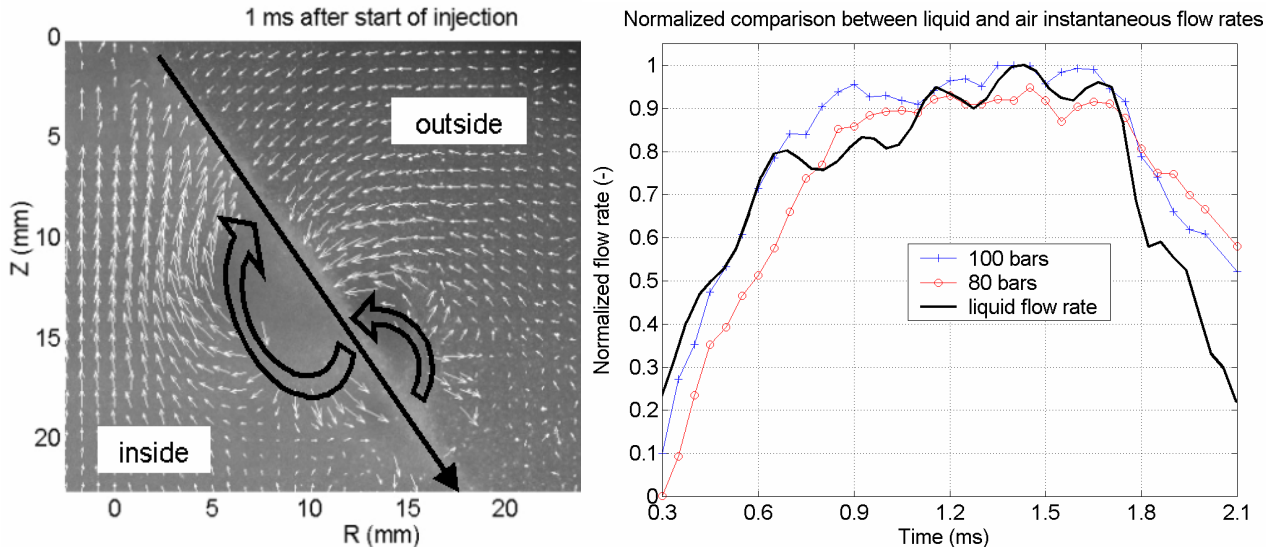

Fig. 1 : GDI injector transient analysis
a) : F-PIV reslts, spray frontier, outer and inner vortices, V_{max}=13 m/s, Injection pressure : 50 bars
b) : Liquid and gaseous instantaneous normalized flow rates

1. INTRODUTION

Assuming that injector instantaneous flow rate has the same shape than its electrical control signal (i.e. a square or a trapezoïd for instance) can be very helpful for a fast, but rough, estimation of gazoline flow rate and pressure gradients magnitude. Indeed, while considering the injector design and the whole fuel system, one has to conclude that more attention has to be paid to many phenomena such as fuel compressibility, pipes elasticity and injector needle motion. As a result, it is necessary to distinguish various sub-systems, having different frequency responses and parameters sensibility. Then, changing the injector design or the fuel system (modifying pipe geometry or materials, as it has been done with the use of common rails) can have a dramatic influence on gasoline instantaneous flow rate and pressure oscillations.

Moreover, the emergence of Gasoline Direct Injection (GDI) concept has induced new constraints for the whole injection system including higher injection pressures (up to 200 bars), shorter injection durations (inferior to 3 ms) and shorter needle lift times (200-300 µs). Considering injection frequencies varying between 10 and 50 Hz (1200-6000 rpm), pressure, and so, flow rate oscillations are no longer negligible even with pressure regulated fuel system.

Thus, we are here presenting instantaneous flow rate results from transient studies dedicated to the quantification of those flow rate oscillations. Various method have been used, the most original being a laser-based instantaneous flow rate rebuilding method (Durst & al. 1996, Bopp & al. 1990, Ismailov & al. (1999, 1999), Durst & al. 1996) inspired from the work of Lambossy (lambossy 1952). Measurements are achieved by Laser Doppler Velocimetry measurements (LDV) at the centerline of a Pyrex pipe mounted before the injector.

To validate these measurements, we have used many experimental methods providing various quantities such as velocity distributions in the Pyrex pipe, mean flow rates (or injected volume) over an injection and of course instantaneous flow rates. Indeed, even if previous studies highlighted very good agreement between laser-based mean flow rates and weightings (Durst & al. 1996, Bopp & al. 1990, Ismailov & al. 1999, 1999, Durst & al. 1996), we have carried out further validations. First, phase-averaged LDV measurements have been achieved to compare velocity distributions in the Pyrex pipe with the rebuilt ones from the centerline velocity. Then, classical weigthings and results from an industrial piston like flowmeter (EMI2, EFS company) have also been used to measure mean flow rates (injected volumes in fact).

Finally, fluorecent particle image velocimetry (FPIV) has also been used to measure the transient motion of the air surrouding the injector all along the injection. After having check mass balance to validate those measurements, we have monitored the transient air entrainment of the spray and compared its fluctuations (magnitude and frequency) to the one measured upstream the injector, in the gasoline system.

2. LASER-BASED INSTANTANEOUS FLOW RATE DETERMINATION

2.1 The Rebuilding Method

This method relies on theoretical principles presented by Lambossy in 1952, who was at that time dealing with blood pressure fluctuations in arteries [2]. It has been then applied to the study of gasoline injectors (Durst & al. 1996, Bopp & al. 1990, Ismailov & al. 1999, 1999, Durst & al. 1996). It is there necessary to consider the general axial component of the Navier-Stokes system for a laminar flow generated in a pipe by an axial pressure gradient (whatever its form) :

$$\frac{\partial U}{\partial t} + U\frac{\partial U}{\partial x} + V\frac{\partial U}{\partial r} = -\frac{1}{\rho}\frac{\partial P}{\partial x} + \upsilon\left(\frac{1}{r}\frac{\partial}{\partial r}\left(r\frac{\partial U}{\partial r}\right)\right) \qquad (1)$$

There, we need to simplify that first equation before going further on. Indeed, the flows we are here considering will be supposed as laminar and parallel ones, these assumptions being discussed later on in this paper. Moreover, a non-dimensionnal analysis approach highlights a critical ratio between unstationary effects (created by injector opening and closing) and viscous ones. There is the Taylor number definition, that can be seen as a length or a time ratio.

$$\frac{U\omega}{\upsilon\frac{U}{R^2}} = \frac{R^2\omega}{\upsilon} = Ta^2 = \frac{R^2/\upsilon}{1/\omega} = \frac{\text{Viscous time}}{\text{Pulse period}} \qquad (2)$$

Thus, for Ta >> 1, the flow is fully parallel, viscous effects being negligible regarding to unstationary ones. It can also be understood by considering the caracteristic times ratio. It indeed indicates that viscous phenomena take far more time to develop than unstationary ones. The phenomena we are here studying will satisfy this criterion (see Validity range) and, thanks to this, (1) can be simplified, becoming (3). This last equation higlights the dependancy of transient effects (LHS) to spatial pressure gradients (RHS1) and viscous effects (RHS2).

$$\rho\frac{\partial U}{\partial t} = -\frac{\partial P}{\partial x} + \mu\left(\frac{1}{r}\frac{\partial}{\partial r}\left(r\frac{\partial U}{\partial r}\right)\right) \tag{3}$$

Up to now, no assumptions have been made concerning the caracteristics of the pressure gradient. Thus, let us consider as a first step an axial pressure gradient composed of a stationary part, p'0, and of only one sinusoidal pressure fluctuation (Eq. 4). The velocity distribution in the pipe (Eq. 5) can be deduced from equation 1 including Taylor's number definition. One can remark that the first term of the right hand side of equation 5 is the same as for a Poiseuille flow whereas the second one delas with more complex velocity distribution, depending on Taylor number.

$$\frac{\partial P}{\partial x} = -\rho\left[p'_0 + (p'_1 e^{i\omega t} + C.C.)\right] \qquad U(r,t) = \frac{R^2 p'_0}{4\upsilon}\left[1-\left(\frac{r}{R}\right)^2\right] + \frac{p'_1}{\omega} ie^{i\omega t}\left[\frac{J_0\left(i^{3/2}Ta\frac{r}{R}\right)}{J_0\left(i^{3/2}Ta\right)}\right] + C.C. \tag{4) (5}$$

Considering only one time-dependant pressure gradient would lead to very poor results, reason why equation 6 takes into account not one, but a sum of sinusoïdal pressure gradients satisfying the following decomposition :

$$\frac{\partial P}{\partial x} = -\rho\left[p'_0 + \sum_{n=1}^{\infty}(p'_n e^{in\omega t} + C.C.)\right] \tag{6}$$

Solving Navier-Stokes equations as for equation 5, the instantaneous velocity distribution inside the pipe is :

$$U(r,t) = \frac{R^2 p'_0}{4\upsilon}\left[1-\left(\frac{r}{R}\right)^2\right] + \sum_{n=1}^{\infty}\left(\frac{p'_n}{n\omega} ie^{in\omega t}\left[\frac{J_0\left(i^{3/2}Ta_n\frac{r}{R}\right)}{J_0\left(i^{3/2}Ta_n\right)} - 1\right] + C.C.\right) \quad (\text{with } Ta_n = R\sqrt{\frac{?_n}{\upsilon}}) \tag{7}$$

Here, again, the Poiseuille stationary term takes part in the final velocity distribution, as well as the "n" first harmonics, all these contributions being weighted with p'0 and p'n coefficients, pressure gradients however still unknown. Once these coefficients evaluated, the instantaneous volumetric flow rate could then be obtain by spatial integration of the velocity distribution. In that way, it is very convenient to consider the instantaneous velocity distribution equation for r=0 (pipe axis). Equation 7 can then be simplified, becoming :

$$U(r=0,t) = \frac{R^2 p'_0}{4\upsilon} + \sum_{n=1}^{\infty}\left(\frac{p'_n}{n\omega} ie^{in\omega t}\left[\frac{1}{J_0\left(i^{3/2}Ta_n\right)} - 1\right] + C.C.\right) \tag{8}$$

One can then remark that the centreline velocity would match very well with the Fourier formalism (eq.9). Indeed this lead to the determination of the unknown pressure gradients thanks to the Fourier coefficients (eq 10a-10b):

$$U(r=0,t) = \frac{c_0}{2} + \sum_{n=1}^{Nexp}\left(c_n e^{in\omega t} + C.C.\right) \qquad \frac{c_0}{2} = \frac{R^2 p'_0}{4\upsilon} \quad \text{and} \quad c_n = i\frac{p'_n}{n\omega}\left[\frac{1}{J_0\left(i^{3/2}Ta_n\right)} - 1\right] \tag{9) (10a-10b}$$

Finally, the flow is spatially and temporally defined, giving access to the instantaneous flow rate by a spatial integration of the velocity distribution and then to the mean flow rate by a temporal integration over the injection period.

2.2 Validity Range

As said before, two conditions have to be fulfilled to lead such an analysis : the laminarity and the parallelism of the flow. In that way, two non-dimensional numbers have to be considered. For the laminarity criterion, we use a Reynolds number. However, it is not based on the Pyrex pipe diameter, as for a steady approach, but on the Stokes' length (eq. 11). This depth caracterizes, for instance, the skin effect of an oscillating plate in a semi-infinite media. In our case, this is not the pipe that is moving, but the fluid, generating this viscous affected area at the vicinity of the wall to fulfill the non-slip condition.

$$Re_\delta = \frac{U\delta}{\nu} \quad with \ \delta = \frac{\sqrt{2\nu}}{\omega} \qquad (11)$$

Frequency (Hz)	1	5	10	20	40	50
δ (10^{-4}m)	7.3	3.3	2.3	1.6	1.2	1
Re_δ	437	195	138	98	69	62

Table 1 : Reynolds number evolution

Many studies have been achieved, experimentally as well as theoretically, and even numerically, dealing with the transition to turbulence of oscillating flows. The most common condition to be found is that flows verifying $Re\delta < 550$ will be laminar ones (Durst & al. 1996, Hino & al. 1976, Wu & al. 1995, David & al. 1991). Considering Pyrex pipe geometry and fluid properties (see Experimental setup paragraph), we can set on the following table dealing with the evolution of Stokes' length (δ) and $Re\delta$ as a function of the injection frequency (table 1).

For a gasoline engine, injection frequency varies from 1 to 50 Hz (engine speed between 1200 and 6000 rpm). We can then conclude that the flows we are considering will be laminar ones ($Re\delta < 550$), the lowest frequencies limiting the validity range as $Re\delta$ decreases with injection frequency.

Concerning the parallelism criterion, i.e. the Taylor number, it raises from 19 to 30 between 2000 rpm and 6000 rpm. Here again, the lowest frequencies are the restrictive ones but the parallelism condition (Ta>1) is always verified and even if the inertia to viscous effects ratio is not actually very high, we will see that this method is still valid. To analyze lower injection frequencies (or pulsation for continuous flows), the use of a pipe with a smaller diameter seems to be the most convenient way, fluid viscosity variation implying too strong modifications of injector internal flows.

2.3 Experimental Setup

Measuring the centerline velocity of the flow feeding the injector is the keystone of the instantaneous flow rate determination. Because of the back flows expected, for instance just after the closing of the injector, a non-intrusive measurement method is required.

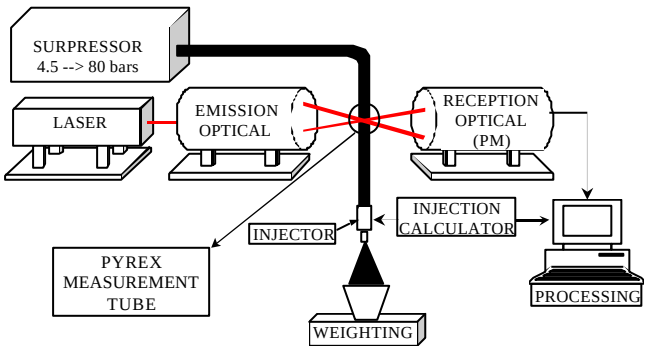

Figure 1 : Experimental set up

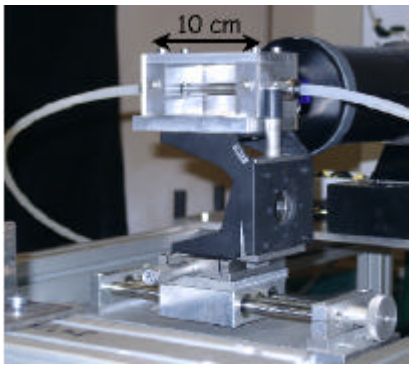

Figure 2 : Pyrex tube mounted on its 3D device

We use a Laser Doppler Velocimetry test bench (fig. 1) equipped with a Spectra Physics continuous laser (Argon 2020, 4W) delivering a 514.5 nm wavelength. The diameter of the ellipsoidal measurement volume is 50 µm and its length is 360 µm. The liquid used is either Stoddard solvent (ρ=763 kg/m3, ν=1.67e-6 m2/s) or ISANE-IP 155 (ρ=747 kg/m3, ν=1e-6 m2/s), seeded with polymer particles (diameter inferior to 5 microns by filtering). Measurements are achieved in a Pyrex pipe (ϕext=12mm, ϕint=4mm) located before the injector and mounted on a 3D displacement device ensuring placement errors inferior to 10 micrometers (figure 2). The hydraulic circuit consists then in a pneumatic surpressor, a 3 meters long flexible, the Pyrex pipe (10 or 50 cm) and the injector. Because of the non-constant time sampling of the rough LDV signal, we use a phase averaging process based on signals provided by the car calculator that drives the injector and the Burst Spectrum Analyzer (DANTEC F60) that collects data. Weighting techniques can be performed at the same time to have a reference for mean flow rate comparisons.

3. VALIDATION OF THE VELOCITY DISTRIBUTION IN THE PYREX PIPE

3.1 LDV Measurements Validation

As LDV measurements are achieved over many injections and then phase averaged, we have checked that the standard deviation for each phase step was inferior to 6%, including shot to shot variations and experimental errors.

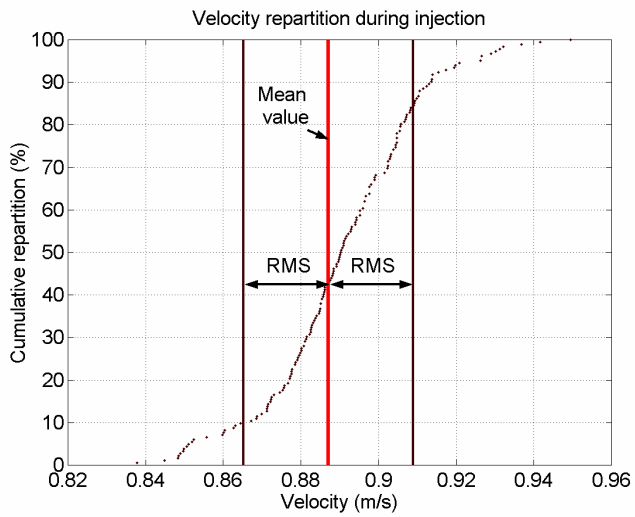

Figure 3 : Velocity histogram

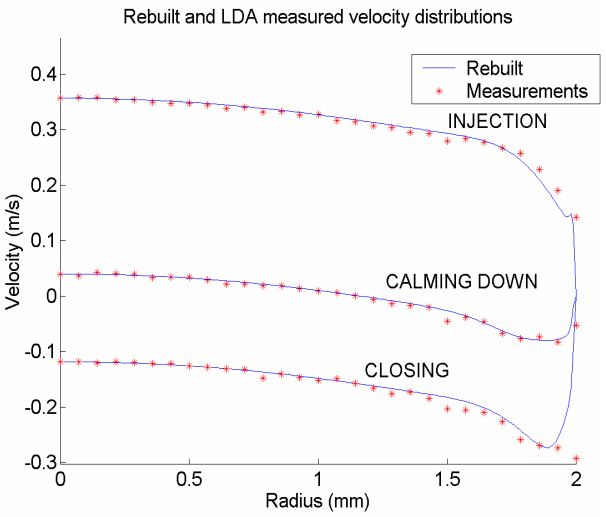

Figure 4 : Velocity distributions by LDV (*) and rebuilding theory (solid line)

Concerning time transit bias for LDV measurements, we have scanned velocity histograms for each phase step. Here again, bias is very low, velocity distribution being symmetrical to its mean value with a quasi-constant slope over a 2 RMS width interval (figure 3). It is here important to stress on time and devices required achieving LDV transient velocity distributions. First of all, every measurement during between 1 and 2 minutes, it takes about two hours to get a spatial and time resolved velocity distribution. Thus, it is critical to have a fair good constant injection pressure source. Furthermore, micrometric displacement system has to be used to ensure a fine motion of the Pyrex pipe, the measurement volume being the reference. Finally, because of various refraction index changes, a law has to be found to fit displacement consigns with the position of the measurement volume in the Pyrex pipe.

3.2 Rebuilt And Measured Velocity Distributions

The best way to validate the rebuilding method is to achieve LDV measurements all along the inner diameter of the Pyrex pipe and to compare them with the rebuilt velocity distributions. As a result, we have chosen three phase steps, that is to say during injection, just after the closing and while oscillations are damping (between two injections). Figure 4 represents the velocity distribution in half the Pyrex pipe. While comparing rebuilt and measured profiles, there is no more ambiguity in the relevance of the rebuilding method. Indeed, whatever velocity direction, magnitude or gradient, there is a very good agreement between the LDV measurements and the rebuilding method. The main gaps are at the vicinity of the wall because of superimposition of the laser measurement volume and of the Pyrex pipe wall. We can here underline that the main advantages of this rebuilding method is that only one measurement is required. We can also notice that the velocity distribution is quite flat at the center of the pipe, and so, even a “rough” localization of the measurement volume at the centerline can lead to quite good results.

4. INSTANTANEOUS FLOW RATE CARACTERISTICS

As a first step, we can have a look at the typical instantaneous flow rate during an injection period (fig. 5). We can catch sight of all the typical events of the injection : injector opening (A), injection (B), injector closing (C) and finally post injection oscillations (D). These fluctuations are due to the equivalent compressibility of the whole system depending on fluid properties but also on pipes and injector designs and materials. We also notice various oscillation frequencies resulting from pressure waves generated in different locations in the hydraulic circuit (various equivalent compressibilities generating different pressure wave celerities). Symmetry of the water hammer effect is also highlighted, opening and closing oscillation being opposite (figure 5).

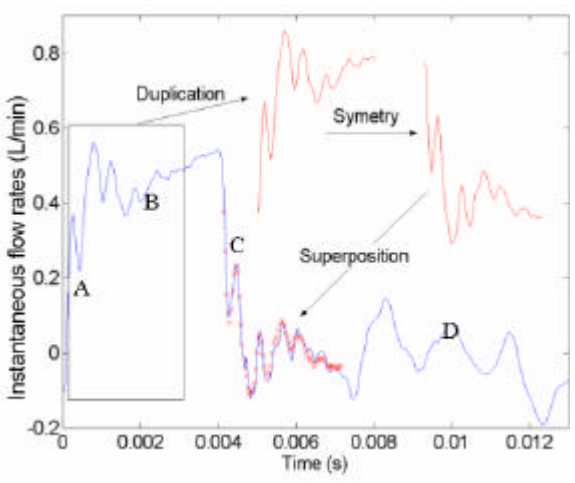

Figure 5 : Instantaneous rebuilt flow rate signal

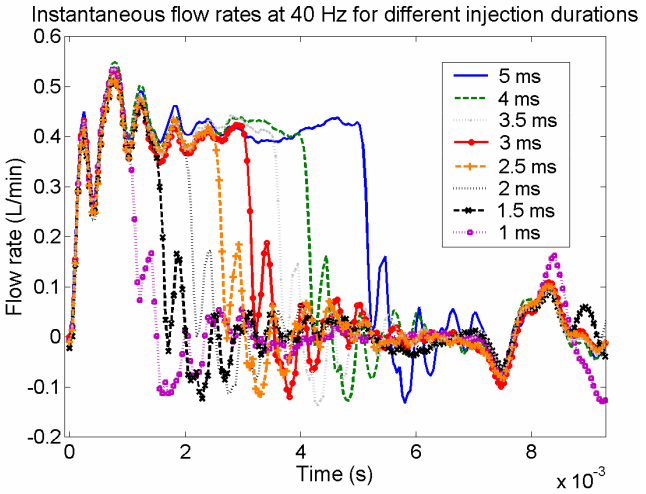

Figure 6 : Return of the opening pressure wave

Finally, we have measured instantaneous flow rate for eight injection durations varying between 1 and 5 ms (figure 6). Remind that, as the injector opens, it generates a pressure wave that travells all along the injector, the pyrex pipe, the gasoline system and then comes back, passing again in the gasoline system and in the measurement pipe. As all openings occur at the same phase (t=0 on figure 6), the return of the pressure wave occurs at the same moment, justifying the quasi-perfect superimposition of flow rate signals some 7.8 ms after the start of injection. The same phenomena, but reversed that time, can also be seen by synchronising injector closing instead of opening

5. FLOW RATE VALIDATION

As flow rate determination is the main interest of this method, we have also compared mean flow rates measured by weightings on one hand, and computed by the rebuilding method on the other. Figure 7 highlights very good agreements between the two methods, whatever the injection frequency or duration. This allows to confirm that even with low injection frequencies, where Re$_\delta$ and Ta are close to their limits, the rebuilding method deviations remain inferior to 5%.

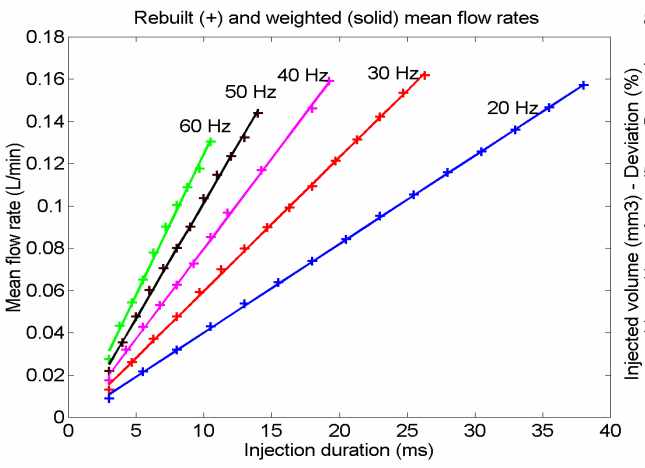

Figure 7 : Weighted (solid lines) and rebuilt (crosses) mean flow rates (various injection durations, frequencies)

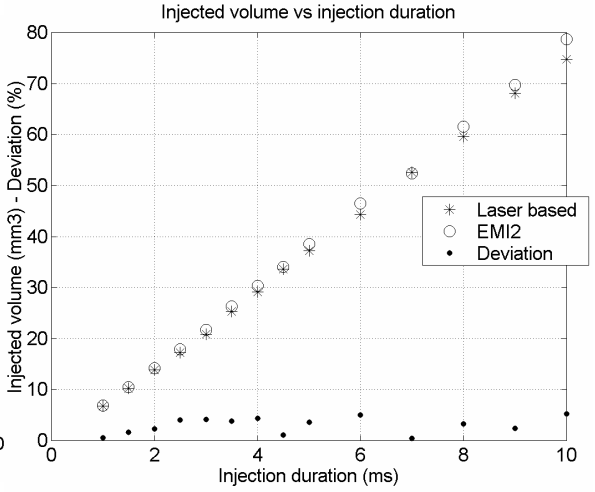

Figure 8 : Comparison between rebuilt (stars) and EMI2 (circles) injected volumes

Even if weighting over numerous injections is a very good way to evaluate mean flow rates, we have also used an industrial piston flowmeter (EMI2, EFS company). It is mounted at the outlet of the injector and is widely used in injectors' calibration. This consists in a liquid-filled piston chamber with a mobile wall moving during the injection. By monitoring its position before and after injection, it is possible to determine the amount of fuel injected and the mean liquid flow rate. Here again, the accuracy of the two methods is verified with deviations inferior to 5% (figure 8).

6.TRANSIENT ANALYSIS OF AIR ENGULFMENT

6.1 Experimental setup - Fluorescent Particle Image Velocimetry

There are many experimental studies that have been carried out on air entrainment generated by diesel or GDI sprays (Lee & Nishida 2003, Rottenkolber & al. 2003, Driscoll 2003, Lisiecki & al. 2003). However, only a few of them deal with its transient analysis and its coupling with instantaneous liquid flow rate, that is our interest here.

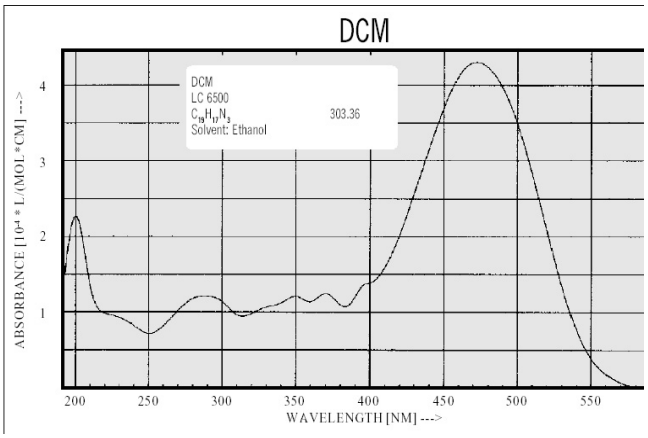

Figure 9 : Absorbance of a DCM-ethanol solution

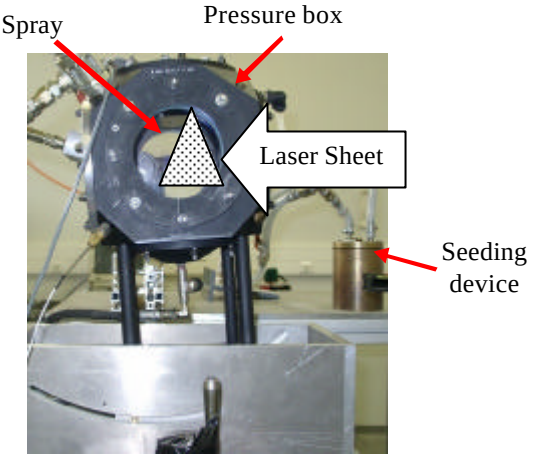

Figure 10 : FPIV bench test

As we want to study the air motion by laser means, we have to keep in mind that the video recorder can be damaged while the laser sheet crosses a dense liquid area. That is why we have decided to use Particle Image Velocimetry on Fluorescent dye (FPIV). Thus, we have designed a dye droplet generator using an air pressurized cylinder with a medical atomizer inside. The mean droplet diameter is slightly inferior to 1 micron with a quite sharp repartition around the mean value (measured achieved with a TSI Aerocinesis Phase Doppler Analyzer).

The liquid used is a propylene carbonate (PC) solution saturated with dichloromethane (DCM), this dye having interesting fluorescent properties. Indeed, when this solution is excited by a Nd YAG laser ($\lambda_{excitation}$ =535 nm) it produces a red-orange fluorescent with a wavelength signal between 615 and 666 nm, maximum efficiency being noticed at $\lambda_{fluorescence}$=639 nm. The absorption spectrum of DCM is presented on figure 9, and even it deals with an ethanol-based solution it gives a good idea of the overall shape of the DCM absorbance.

Concerning the experimental setup, we have used a Spectra Physics laser (ND-YAG PIV 2*400, 535 nm) as an excitation source. The intensified numerical video recorder used is a Sensicam QE that has a resolution of 1040*1376 pixels. A red filter (OG 590 nm) is placed to make the camera “blind” to the diffusion of the laser sheet by the spray.

However, because of the poor energy of the fluorescence signal, we use a 2 per 2 pixels bining, reducing the resolution of the camera to 520*688 but virtually increasing the sensor sensibility. The size of the fields is close to 25*30 mm and only the half of the air velocity field around the spray can be visible. The PIV algorithm is a multigrid inter correlation based one with subpixel cell shifting. Interrogation cells size is 16*16 pixels, the actual size of PIV cells being then 700*700 micrometers.

We have used a pressure box (no back pressure sensibility being however investigated in this paper) equipped with optical accesses to study spray development and air motion (fig. 10). The injector feeding system is exactly the same as the one mentioned in the instantaneous flow rate study to be able to achieve comparisons between liquid flow rate oscillations and entrained air ones. The synchronization of laser pulses, video recorder gates and injection is performed by two computers and the car calculator that drives injection frequency and duration. The delay between two laser pulses is not fixed as the spray has a ten time faster dynamic than the air. This is due to the progressive entrainment of the air as the spray penetrates. Typical values for this delay are varying between 50 and 10 microseconds and the spray and velocity field are monitored with a 50 microseconds time step.

6.2 Spray and air images

By looking at images used for FPIV (figure 11) we have noticed that, contrary to what was expected, the spray is still visible because of two phenomena. First, the liquid injected (Stoddart solvent or Isane IP155) also produces a fluorescence signal. Then, there is also spray Mie scattering of dye fluorescent emission. This can be clearly seen on gray level histogram clearly highlighting three peaks (figure 12). The lower one comes from image background (noise), while the second one is the "usefull" one in fact, coming from fluorescent dye signal. Finally, the spray Mie scattering is the last peak, these analysis having been validated by achieving local gray level histograms first away from the spray (background+dye) and then following spray frontier (spray Mie scattering).

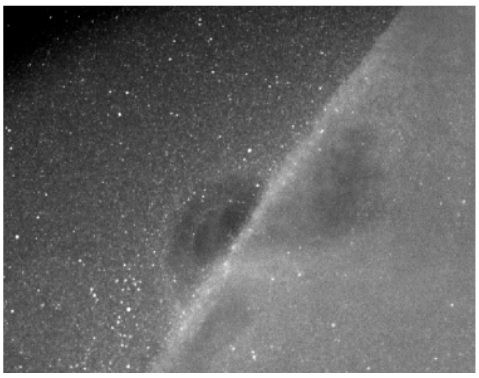

Figure 11 : FPIV dedicated image

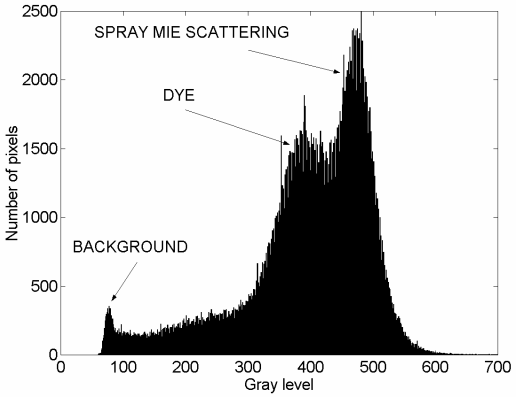

Figure 12 : Gray level histogram

As a result, the spray is visible that can be in fact quite a good thing to notice spray penetration, frontier and vortices. However, it is sometimes impossible to analyze the internal spray structure when density of the spray increases, that is to say for high needle lift or when injection pressure is superior to 50 bars (figures 13 a, b ,c ,d ,e ,f). This can be due to laser sheet diffusion on the spray or injected liquid fluorescence. It could be possible to investigate the air inside by splitting the original laser sheet. One sheet analyses the external of the spray and the other one comes from under the spray to get the internal part of the spray from the same realization, being attentive to the fact that repetitive impingements of the laser sheet on the injector could damage it.

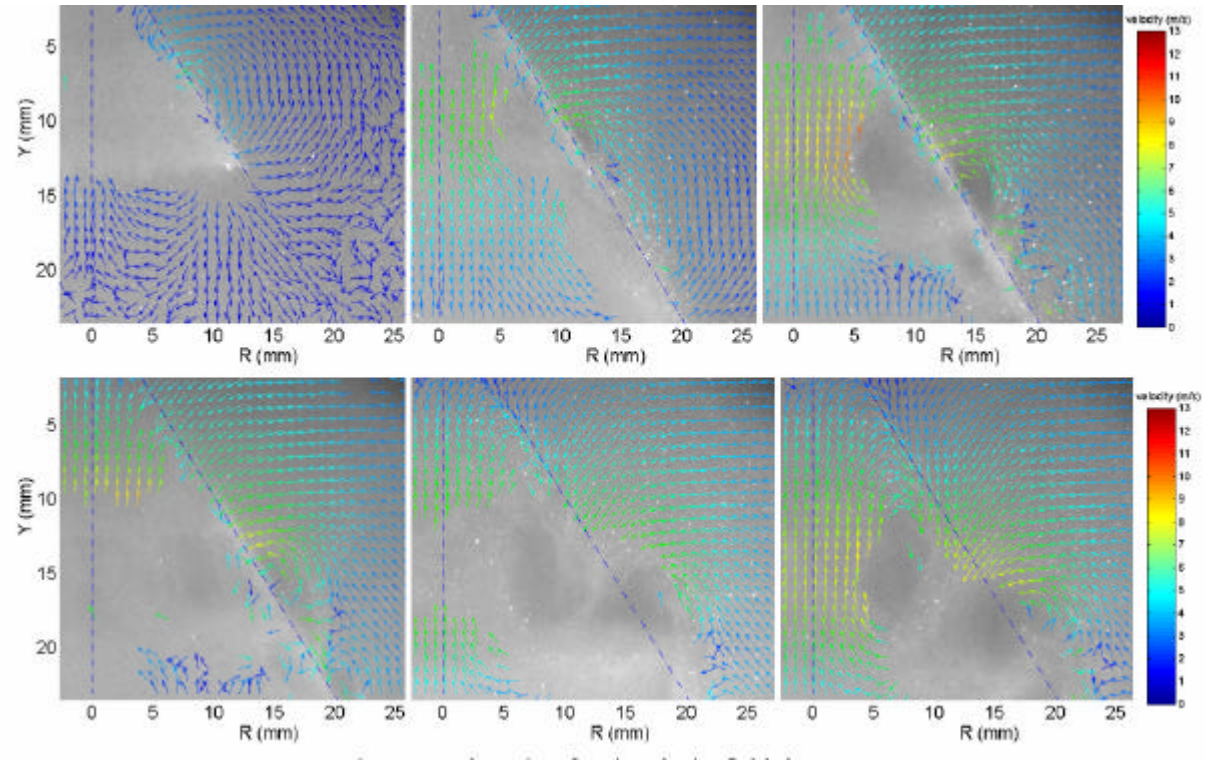

Figure 13 a, b, c, d, e, f : Air velocity fields by FPIV
0.3, 0.6, 1, 1.1, 1.4, 1.6 ms after start of a 1 ms injection (50 bars injection pressure)

The structure of the spray is a thin conic layer (about 1 mm) composed of liquid droplets. There are only a very few droplets inside the spray, apart from those convected by the inner vortex. Indeed, because of the shear layer produced by the spray motion in the air at rest, vortices are generated on both sides of the spray. In fact, there are pairs of vortices that are generated but the ones appearing inside the spray are far more intensive and large than the external ones. Moreover, there is always one part of the initial spray sheet that continues without any bending in comparison with its original angle (half cone angle close to 40°). Finally, because of the air friction, the droplet layer is getting thicker as it penetrates. In spite of the spray image on pictures background, PIV algorithm is efficient and correlates only on the dye. Indeed, even if the laser sheet is illuminated, it is too dense to be analyzed. Concerning the lack of data in vortices area, it can be due to the fuel dropplet vortices that blurs images.

While considering the outside of the spray, one can notice that air is slowly entrained to have a final vortex-like motion around outer vortices, coming from the bottom of the spray to the top. As a result, the part of the spray that actually entrains the air is located in the near region of the nozzle, before the main vortices, here for penetration lengths inferior to 13 mm. The typical external velocity magnitudes close to the spray varies from 3 to 8 m/s for injection pressures between 50 and 100 bars. The internal air motion is a high intensity ascendant air flow, generated by the inner vortex. However, velocities close to the internal spray frontier are about 40% higher than the external ones.

6.3 Validation

Before any further analysis, we have checked the mass conservation law over a square section tore located at the outside of the spray (area defined on figure 14, experimental results on figure 15). As the spray has not penetrated the control area, the mass balance gap remains high because of the residual 3D motion of air at rest (delay after start of injection < 150 µs). As soon as the spray tip has reached the bottom of the control area, gaps remain close to 10%, even after injection. Let us notice that there is no swirl motion for the injector investigated in this case, reducing the three-dimension motion of the spray and so of the air.

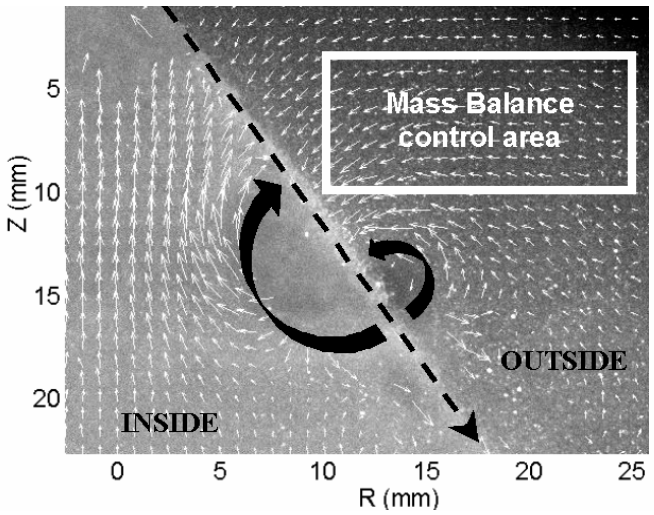

Figure 14 : Spray geometry and air motion
(maximum velocity : 9m/s, Pinj = 50 bars, pw = 1 ms)

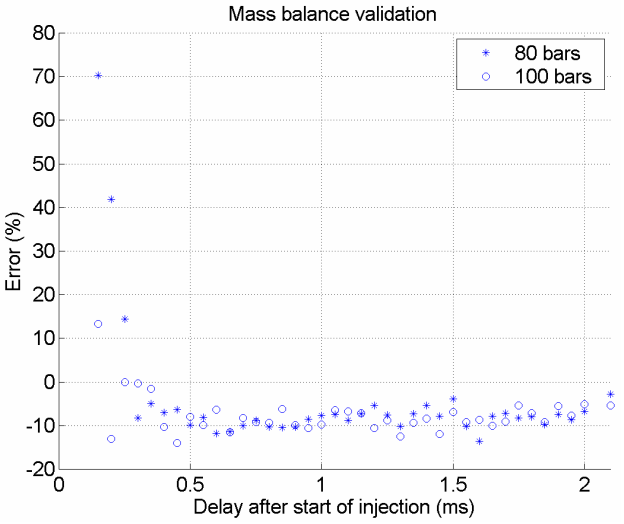

Figure 15 : Mass balance gap over an injection period

7. LIQUID AND AIR FLOW RATES COUPLING

To evaluate the instantaneous air flow rate entrained by the spray, we have integrated the velocity field perpendicularly to the external frontier of the spray and on its whole circumference. Measurement are located about 500 microns from the spray to be as relevant as possible, smallest distance leading too often to wrong air velocity calculations. Then, we can compare transient evolution of instantaneous flow rates, the liquid one being measured by the rebuilding method and the gaseous one by FPIV. As it takes some time for the fluid to move from the middle of the Pyrex pipe to the outlet of the spray, the instantaneous liquid flow rate curve has been delayed in comparison with the gaseous one (fig. 16). By comparing liquid and gaseous instantaneous flow rates evolutions, it is possible to highlight many similarities.

Mean slopes at the opening and at the closing are quite close for each curve even if we can notice slope variations for the liquid flow rate**.** This is because we are not measuring the liquid flow rate at the outlet of the injector but in the middle length of the Pyrex pipe. We are still working to determine the transfer functions of the injector and of the circuit to get the right liquid flow rate at the outlet. Indeed, a perfect square signal at the extremity of a pipe (here generated by the opening and closing of the injector) becomes different at the middle by a temporal delay and a magnitude modulation.

Concerning air and liquid oscillations during injection, one can consider that they are quite well correlated considering their frequencies and magnitudes. However, and as it can be expected, the maximum to minimum flow rate ratio is more significant for the liquid than for the air because of damping of liquid oscillations while passing through the injector and spreading into the air.

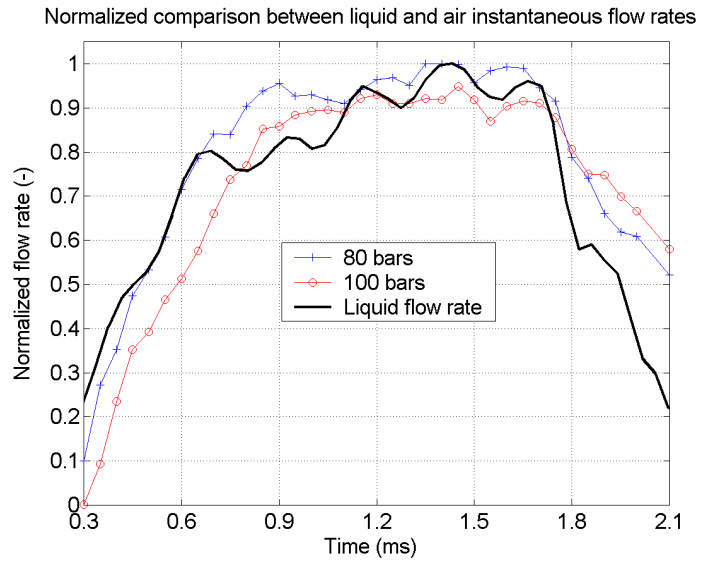

Figure 16 : Liquid and gaseous instantaneous flow rates

8. CONCLUDING REMARKS

The rebuilding method we have used here is very well suited to the study of periodical pulsed flows that can be found in alternative or continuous engines (where the flow can be pulsed by combustion instabilities). Up to now, it has been validated on mean criteria (flow rates, velocity distributions) but is up to be done for instanaeous flow rate (Delay & al. 2004).

Depending on hydraulic circuit considered, we have noticed that oscillation magnitude can reach up to 40 % of the static flow rate of the injector. However, these values have been found for low pressure indirect injector being fed by very flexible hoses. High pressure systems leads to smaller but still significant oscillations (only 10 % of the static value). As the rigidity of the circuit increases, oscillation frequencies increase as well but still depending on the length of the whole hydraulic system. There is still to establish the transfer function that will computes the flow rate at the outlet of the injector from the one at the middle length of the measurement pipe.

We have also begun to highlight a dependency between upstream liquid oscillations and downstream gaseous ones. Indeed, the same frequencies can be found in each flow rate transient evolution and magnitudes seem to follow that trend. So, this work has to be continued to investigate the effect of injection pressure, injection duration and back pressure, and to purpose a transient air entrainment model based on integral models (Cossali 2001).

9. NOMENCLATURE

δ : Stokes' length (m)
ϕ_{ext}, ϕ_{int} : outer, inner pipe diameter (m)
$\lambda_{excitation}$: laser wavelength (nm)
$\lambda_{fluorescence}$: dye fluorescence wavelength (nm)
ν : kinematic viscosity (m^2/s)
ρ : density (kg/m^3)
ω : pulsation (rad/s)

c_o, c_n: Fourier coefficients
C.C. : complex conjugate
F : injection frequency (Hz)
J : Bessel function
P : pressure (bar)

Pinj : injection pressure (bar)
pw : pulse width ≈ injection duration (ms)
R : pipe radius (m)
r : radial coordinate (m)
$Re_?$: Reynolds number based on Stokes' length (-)
t : time (s)
Ta : Taylor number (-)
U : axial velocity (m/s)
x : axial coordinate (m)

10. REFERENCES

Durst, F., M. Ismailov, et al. (1996). "Measurement of instantaneous flow rates in periodically operating injection systems."Experiments in fluids 20: 178-188 ;

Lambossy, P. (1952). "Oscillations forcées d'un liquide incompressible visqueux dans un tube rigide et horizontal. Calcul de la force de frottement.Helvetica Physiol. Acta, 371-386, 1.II.1952.

Bopp. S., Durst, F., Teufel M. and Weber H.. (1990). "Volumetric flow rate measurements in oscillating pipe flows with a laser Doppler sensor.". Measurement science and technology, 1, : 917-923.

Ismailov M., Durst, F and Obokata T. (1999). "LDV flow rate measurements applied for analysis of transient injection characteristics.". JSME international journal. Series B, fluids and thermal engineering, vol 42, n°1 , 22-29.

Ismailov M., Ishima T., Obokata T., Tsukagoshi M. and Kobayashi K. (1999). "Visualization and measurements of sub-millisecond transient spray dynamics applicable to direct injection gasoline engine (Part 3 : Measurements of instantaneous and integrated flow rates in high pressure injection system using LDV-based meter)". JSME international journal. Series B, fluids and thermal engineering, vol 442, n°1 , 22-29.

Durst, F., Melling A., Trimis, D. and Volkholz P. (1996). "Development of a flow meter for instantaneous flow rate measurements of anaesthetic liquids.". Flow measurement instrumentation, vol. 7, n° ¾ : 215-221.

Hino, M., M. Sawamoto, et al. (1976). *« Experiments on transition to turbulence in an oscillatory pipe flow. »*. Journal of Fluid Mechanics 75 (2): 193-207

Wu, X., Lee, S. S. et Cowley, S.J. (1995). *« On the weakly nonlinear three-dimensional instability of shear layers to pairs of oblique waves : the Stokes layer as a paradigm. »*. Journal of Fluid Mechanics 253: 681-721

David M. Eckmann et James B. Grotberg (1991). *« Experiments on transition to turbulence in oscillatory pipe flow. »*. Journal of Fluid Mechanics 222 : 329-350

Lee, J., Nishida, K. (2003). *« Simultaneous flow field measurement of DI gasoline spray and entrained air by LIF-PIV technique. »* SAE technical papers series 2003-01-1115. World congress, Detroit, March 2003.

Rottenkolber, G. et al. (2003). *"Combined PDA and LDV measurements : phase discrimination inside a spray using fluorescent seeding particles"*. ICLASS 2003 proceedings, Sorento, Italy

Driscoll, K.D., Sick, V., Gray, C. (2003). *"Simultaneous air/fuel-phase PIV measurements in a dense fuel spray"*. Experiments in fluids 35 (2003) pp. 112-115.

Lisiecki, D., Gobin, C., Ledoyen, S., Ledoux, M. (1998). "The structure of the air flow entrained by a high *pressure diesel jet"*. ILASS Europe 99 proceedings, Toulouse, France.

Delay, G & al. (2004). "*Coupling between instantaneous liquid flow rate and transient air entrainment for GDI sprays*". 3rd International Symposium on Two-Phase Flow Modeling and Experimentation,Pisa, 22-24 September 2004

Cossali, G. E. (2001). "*An integral model for gas entrainment into full cone sprays"*. J. Fluid Mech., vol 439, pp.356-366.